THE JOURNAL OF PHYSICAL CHEMISTRY Letters

Letter

Cite This: J. Phys. Chem. Lett. 2017, 8, 6135−6141

pubs.acs.org/JPCL

# High-Throughput Computational Screening of Multivariate Metal−Organic Frameworks (MTV-MOFs) for $CO_2$ Capture

Song Li,[†] Yongchul G. Chung,[‡] Cory M. Simon,[§] and Randall Q. Snurr*[,∥]

[†]State Key Laboratory of Coal Combustion, School of Energy and Power Engineering, Huazhong University of Science and Technology, Wuhan 430074, China

[‡]School of Chemical and Biomolecular Engineering, Pusan National University, Busan 46241, Korea (South)

[§]School of Chemical, Biological, and Environmental Engineering, Oregon State University, Corvallis, Oregon 97331, United States

[∥]Department of Chemical and Biological Engineering, Northwestern University, Evanston, Illinois 60208, United States

Supporting Information

**ABSTRACT:** Multivariate metal−organic frameworks (MTV-MOFs) contain multiple linker types within a single structure. Arrangements of linkers containing different functional groups confer structural diversity and surface heterogeneity and result in a combinatorial explosion in the number of possible structures. In this work, we carried out high-throughput computational screening of a large number of computer-generated MTV-MOFs to assess their $CO_2$ capture properties using grand canonical Monte Carlo simulations. The results demonstrate that functionalization enhances $CO_2$ capture performance of MTV-MOFs when compared to their parent (unfunctionalized) counterparts, and the pore size plays a dominant role in determining the $CO_2$ adsorption capabilities of MTV-MOFs irrespective of the combinations of the three functional groups (−F, $-NH_2$, and $-OCH_3$) that we investigated. We also found that the functionalization of parent MOFs with small pores led to larger enhancements in $CO_2$ uptake and $CO_2/N_2$ selectivity than functionalization in larger-pore MOFs. Free energy contour maps are presented to visually compare the influence of linker functionalization between frameworks with large and small pores.

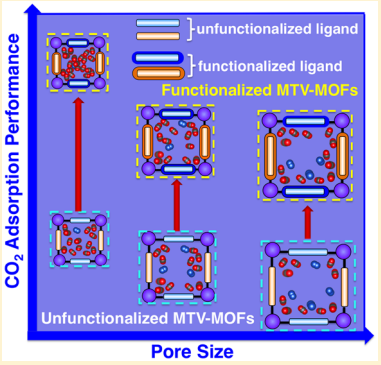


Metal−organic frameworks (MOFs) have received great attention in recent years as potential adsorbents for gas separation due to their unique properties, including extremely large surface area, high porosity, facile tunability, and structural diversity.[1] Most MOFs reported to date consist of one type of inorganic node and one type of organic linker. However, paddlewheel MOFs with two types of linkers have been known for many years,[2,3] and a wider variety of mixed-component MOFs with different linkers, metals, or functionalities have been reported more recently;[4] for example, multivariate (MTV)-MOFs reported by Deng and co-workers are synthesized based on a variety of organic linkers[5] and/or metal nodes.[6] The tremendous structural diversity of MTV-MOFs greatly expands the total number of possible MOFs and increases the possibility of discovering high-performing MOFs for environmental applications, such as $CO_2$ capture.

It has been reported that the properties of MTV-MOFs are not simple, linear combinations of the properties of monolinker MOFs.[1] Deng and co-workers found a MTV-MOF that exhibited a 4-fold enhancement in its $CO_2/CO$ selectivity compared with its best monolinker counterpart from 18 synthesized multivariate MOF-5 analogues.[5] The discovery led to growing research interest in the synthesis of MTV-MOFs. Solid-state nuclear magnetic resonance (NMR) measurements show that different spatial distributions (i.e., random, alternating, and clustered) of functional groups arise in MTV-MOFs.[7] These arrangements are influenced by interactions between the functional groups.[1] Further, the distribution of functional groups was shown to affect gas adsorption.[7] Katzenmeyer and co-workers adopted a more direct approach, the photothermal induced resonance (PTIR) technique, to identify the heterogeneous and homogeneous domains of MTV-MOFs in high resolution.[8] Recently, the detailed arrangement of functionalities inside of frameworks was also investigated by integrated experimental and computational studies.[9,10] Modeling and computation play important roles in revealing the origin of the enhanced adsorption performance in MTV-MOFs. For example, Han et al. attributed the higher $CO_2$ uptake in a functionalized MTV-MOF (i.e., MOF-5-$NO_2$−$NH_2$) predicted from grand canonical Monte Carlo (GCMC) simulations to the enhanced electrostatic interaction with linkers and the tighter geometry given by the smaller pore volume.[11] Similarly, the increased $CO_2$ uptake observed in MTV-MOFs functionalized by two different amino acid (AA) side chains was also ascribed to the $CO_2$−AA interaction in computational work by Drummond et al.[12] A molecular simulation study by McDaniel and co-workers elucidated that

**Received:** October 12, 2017
**Accepted:** December 5, 2017
**Published:** December 5, 2017




DOI: 10.1021/acs.jpclett.7b02700
J. Phys. Chem. Lett. 2017, 8, 6135−6141

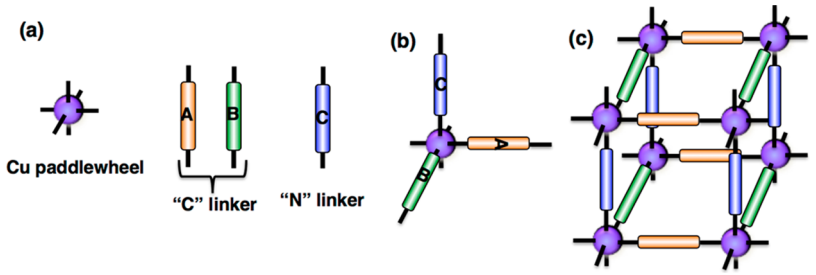


**Figure 1.** Database of functionalized MTV-MOFs consisting of three different types of organic linkers with copper paddlewheel nodes. (a) A (in orange) and B linkers (in green) are terminated with carboxylate groups ("COO" linkers), and C linkers (in blue) are terminated with nitrogen atoms ("N" linker). The arrangement of A, B, and C linkers is shown in (b) with a molar ratio of A:B:C = 1:1:1. A schematic MTV-MOF in **pcu** topology is shown in (c). Note that A ≠ B ≠ C for all functionalized MTV-MOFs, whereas for their corresponding unfunctionalized counterparts, in some cases A = B.

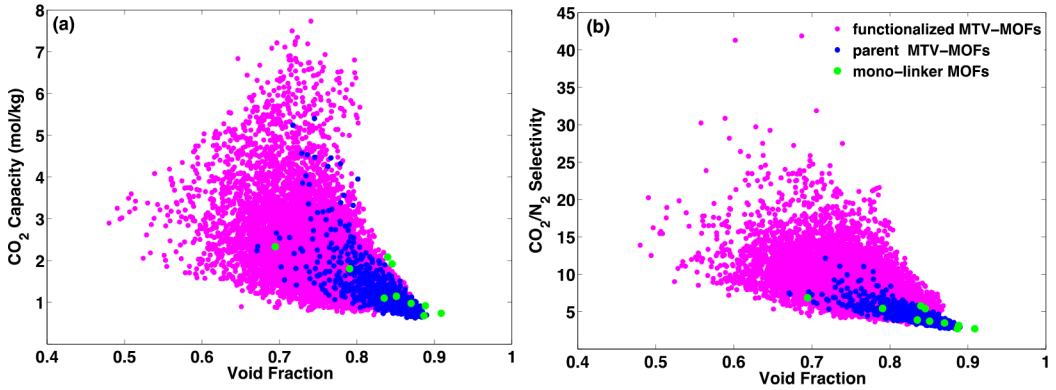


**Figure 2.** Comparison of (a) $CO_2$ adsorption capacity and (b) $CO_2/N_2$ selectivity of monolinker MOFs, parent MTV-MOFs, and functionalized MTV-MOFs in relation to the void fraction. The $CO_2$ adsorption capacities were predicted from GCMC simulations of single-component adsorption at 298 K and 1 bar. Selectivities were calculated from binary GCMC simulations of a gas-phase composition of 10% $CO_2$ and 90% $N_2$ at 298 K and 1 bar total pressure.

the enhancement of adsorption in mixed-linker MOFs originated from the synergistic interactions of adsorbates with multiple linkers.[13]

Although the conventional one-pot synthesis strategy works well for MTV-MOFs consisting of different linkers of the same length,[5,7,14] MTV-MOFs with mixed linkers of varying lengths are more difficult to synthesize by a one-pot synthesis strategy.[15−17] To overcome this challenge, Yuan and co-workers developed a novel "sequential linker installation" approach enabling precise positioning of functional groups in mixed-linker MTV-MOFs,[15] opening a new opportunity in the development of improved MTV-MOF adsorbents.

In addition to synthetic challenges, another challenge is to predict which combination of linkers for a MTV-MOF will synergistically yield a top performer. Due to the ability to choose multiple linkers, the very large, combinatorial number of possible MOFs is intensified for MTV-MOFs. High-throughput computational screening, whereby structure models are built on a computer and molecular simulations are subsequently carried out to rapidly evaluate the performance of generated structures, has been successfully employed for selecting high-performing MOF candidates for $CO_2$ capture,[18,19] $SO_2$ and $NO_x$ separation from flue gas,[20] methane[21] and hydrogen[22] storage, and noble gas separation.[23,24] By predicting a performance ranking of materials prior to synthesis, such high-throughput computational screening can focus experimental efforts on the most promising candidates. This provides a practical means to accelerate the discovery of high-performing materials from a large number of possible MTV-MOFs. However, for MTV-MOFs, the identification of structure−property relationships is complicated because of the lack of performance data for a large number of MTV-MOFs with diverse structural features. In this work, we systematically generated ∼10 000 hypothetical MTV-MOF structures and conducted high-throughput computational screening of these materials for $CO_2$ capture. By analyzing the performance data, we reveal insights into the dependence of functionalization-enhanced $CO_2$ capture performance on the pore size of the MOFs. To the best of our knowledge, this is the first *in silico* screening study of MTV-MOFs.

We constructed 10 995 MTV-MOFs with mixed, functionalized linkers and 560 of their unfunctionalized parent counterparts, consisting of 490 three-linker MOFs and 70 two-linker MOFs. For construction of the functionalized MTV-MOF database, we first selected 20 organic linkers that can be functionalized and 1 unfunctionalizable linker that could form a MOF with **pcu** topology with copper paddlewheel nodes (Figure 1). For the linker selection, we only selected linkers that are not too bulky, with the aim of avoiding steric hindrance with neighboring linkers. Our approach to construct the structures was based on a previously reported method by Wilmer and co-workers,[21] but we eliminated the random functionalization step and instead prepared functionalized linkers prior to MOF construction. To achieve the highest degree of surface heterogeneity, each functionalized MTV-MOF consisted of three different linkers, with three functional groups of varying sizes: −F, $-NH_2$, and $-OCH_3$. For comparison, 10 "monolinker" MOFs were also constructed using the unfunctionalized linkers, where the carboxylate and


DOI: 10.1021/acs.jpclett.7b02700
J. Phys. Chem. Lett. 2017, 8, 6135−6141

nitrogen-terminated linkers contained the same central backbone (e.g., linker 6C with linker 4N in Figure S1). All MTV-MOFs of **pcu** topology that we generated exhibited an alternating spatial distribution of functionalities in the frameworks (as shown in Figure 1) to maximize synergistic effects that may arise (i.e., linkers of a given type are not clustered). See the Supporting Information (SI) for more details about the database generation.

Following the MTV-MOF database generation, we screened the database using grand canonical Monte Carlo simulations to investigate the advantage of combining multiple linkers in constructing MOFs for $CO_2$ capture. Figure 2 shows the $CO_2$ capacity and $CO_2/N_2$ selectivity for the monolinker MOFs, the parent (unfunctionalized) MTV-MOFs, and the functionalized MTV-MOFs. The comparison between the monolinker MOFs (green) and parent MTV-MOFs (blue) shows that higher $CO_2$ capacity and $CO_2/N_2$ selectivity can be achieved by introducing an additional type of organic linker into these MOFs. More importantly, comparison of the parent (blue) and functionalized (pink) MTV-MOFs shows that both $CO_2$ capacity and $CO_2/N_2$ selectivity are further improved by functionalization of linkers. This is consistent with experimental observations of improved performance in monolinker MOFs upon functionalization,[25,26] in which both Zr-NDC[25] and ZIFs[26] consisting of functionalized organic linkers exhibit enhanced $CO_2$ uptake and increased selectivity toward $CO_2$ compared with their unfunctionalized counterparts. Selected top-performing functionalized MTV-MOFs are shown in Figure S3, including the MOFs exhibiting the highest $CO_2$ capacity, the highest $CO_2/N_2$ selectivity, and the most significant enhancement in their $CO_2$ capacity or $CO_2/N_2$ selectivity upon functionalization. Figure 2 also shows that the void fraction generally decreases with functionalization due to the additional space occupied by replacing hydrogen with bulkier functional groups.

On the basis of the data generated from the screening, the MTV-MOF database can provide insight into whether the pore shape and size of a MOF or specific functional groups are responsible for the improvement of the $CO_2$ capture performance in functionalized versus unfunctionalized MOFs. In regard to the pore shape, because all MTV-MOFs in this work exhibit **pcu** topology, if all three linkers of a MOF have a similar length, the pore has a cubic shape, and if the variance in the lengths of the three linkers is large, the pore has a cuboid shape. We find that MTV-MOFs with cuboid-shaped pores exhibit both higher $CO_2$ adsorption capacity and higher $CO_2/N_2$ selectivity than the ones with cube-shaped pores (Figure S4). To understand whether this enhancement originates from the pore shape or from the presence of specific functional groups in the frameworks that are correlated with the linker lengths, we categorized the structures in the MTV-MOF database into 16 groups according to the combination of functional groups (Table 1). Each functionalized MTV-MOF is composed of three types of linkers, and each linker carries one type of functional group (i.e., three types of functional groups in total), except linker 1C, which cannot be functionalized (Figure S1). Note that only the combination—not the permutation—of three functional groups defines the combination type. For example, $NH_2$−F−$OCH_3$, F−$NH_2$−$OCH_3$, $OCH_3$−F−$NH_2$, and $NH_2$−$OCH_3$−F are equivalent combination types. Therefore, there are 10 possible combinations of functional groups for MOFs consisting of three types of functionalized linkers and six for MOFs consisting of two functionalized linkers and the one unfunctionalizable linker 1C. Note that linker 1C is also the shortest among the 21 linkers used for the database construction.

**Table 1. Combinations of Functional Groups in the MTV-MOF Database**

| combination type | functional group combination | # of MOFs |
|---|---|---|
| 1 | F−F−F | 420 |
| 2 | $NH_2$−$NH_2$−$NH_2$ | 420 |
| 3 | $OCH_3$−$OCH_3$−$OCH_3$ | 256 |
| 4 | F−$NH_2$−$OCH_3$ | 2379 |
| 5 | F−$NH_2$−$NH_2$ | 1330 |
| 6 | F−$OCH_3$−$OCH_3$ | 1002 |
| 7 | $NH_2$−$OCH_3$−$OCH_3$ | 991 |
| 8 | $NH_2$−F−F | 1330 |
| 9 | $OCH_3$−F−F | 1158 |
| 10 | $OCH_3$−$NH_2$−$NH_2$ | 1158 |
| 11 | F−F | 70 |
| 12 | $NH_2$−$NH_2$ | 70 |
| 13 | $OCH_3$−$OCH_3$ | 45 |
| 14 | F−$NH_2$ | 140 |
| 15 | F−$OCH_3$ | 113 |
| 16 | $NH_2$−$OCH_3$ | 113 |

In order to explore the correlation between the adsorption performance and the combination of functional groups, Figure 3 presents the $CO_2$ capture performance for the MTV-MOFs grouped by their functional group combination types. Generally, MTV-MOFs of types 1−10 exhibit significantly lower $CO_2$ uptake (Figure 3a) and slightly lower $CO_2/N_2$ selectivity (Figure 3b) than those of types 11−16. Similarly, types 11−16 have higher $CO_2$ heats of adsorption than types 1−10 (Figure 3c), explaining the tendencies observed in Figure 3a,b. Figure 3d summarizes the largest cavity diameters (LCDs) of the MTV-MOFs according to their functional group combination types. MOFs of types 1−10 tend to have larger pores than those of types 11−16. Recall that all MTV-MOFs of types 11−16 contain the shortest linker 1C in their frameworks, which is the limiting length determining the pore size. According to previous experimental and theoretical studies based on monolinker MOFs, smaller pore size is beneficial for improving adsorption separation performance of MOFs,[18,26] which is consistent with the results for mixed-linker MTV-MOFs from this work. Taking these results into consideration, the underlying reason that the MTV-MOFs of types 11−16 with cuboid-shaped pores show significantly better $CO_2$ capture performance than those with cube-shaped pores is likely the smaller pore size of the MOFs with cuboid-shaped pores. The analysis also suggests that, while the specific combination of functional groups may play an important role in some cases in determining the $CO_2$ capture performance of MTV-MOFs, the pore size also plays an important, sometimes dominating, role.

Another way to classify the MTV-MOFs is according to the 560 families of parent structures. Figure 4 shows the average $CO_2$ capacity and $CO_2/N_2$ selectivity of the 560 families of functionalized MTV-MOFs plotted against those of their parent counterparts without any functionalization. The results show that, in each family, every functionalized derivative exhibits better $CO_2/N_2$ selectivity than its parent counterpart and all of the functionalized derivatives show higher $CO_2$ capacity than their parent structures, except the seven MTV-MOFs of types 13, 15, and 16 with LCDs between 5 and 6.5 Å that are shown in Table S1. The underlying reasons are 2-fold: (i) $CO_2$ adsorption in small pores could be already saturated at 1 bar



DOI: 10.1021/acs.jpclett.7b02700
J. Phys. Chem. Lett. 2017, 8, 6135−6141

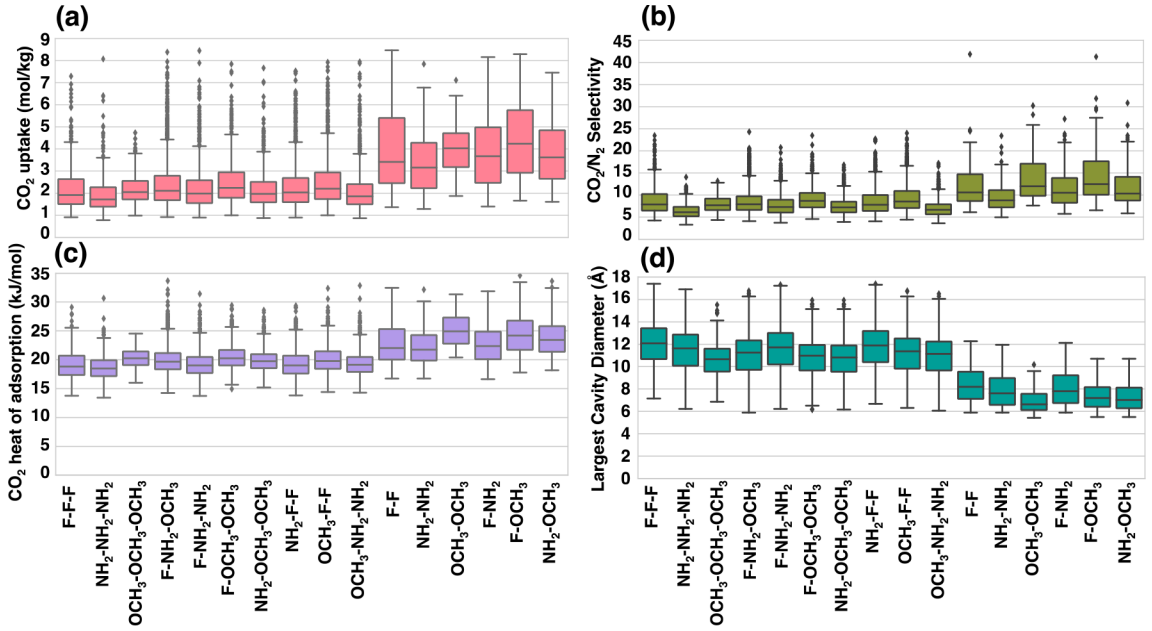


**Figure 3.** Boxplots of (a) $CO_2$ uptake, (b) $CO_2/N_2$ selectivity, (c) $CO_2$ heat of adsorption, and (d) LCD of each group categorized based on the combination type of functional groups in our MTV-MOF database. The $CO_2$ uptake and selectivity were calculated as in Figure 2. The $CO_2$ heat of adsorption was calculated at 1 bar and 298 K. The horizontal line in the rectangular box denotes the median value of the group. The lower and upper boundaries of the rectangular box represent the lower (first quartile or Q1) and upper (third quartile or Q3) hinge, respectively. The lower and upper bars represent the lower (minimum, which is calculated as Q1 − 1.5 × the interquartile range (IQR) that spans the first quartile to the third quartile range (IQR = Q3 − Q1)) and upper (maximum, which is calculated as Q3 + 1.5 × IQR) fence, respectively. The points above or below the upper and lower fence are considered outliers, which are more than three times the IQR above the third quartile or below the first quartile.

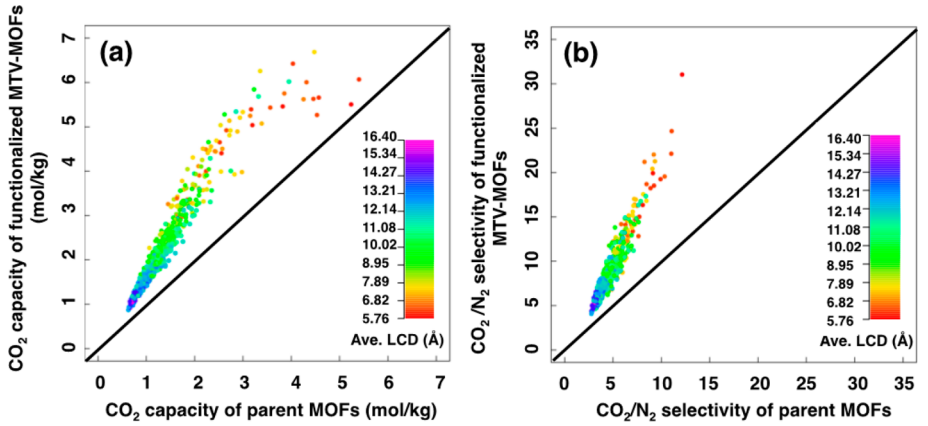


**Figure 4.** Average (a) $CO_2$ capacity and (b) $CO_2/N_2$ selectivity of 560 families of MTV-MOFs versus those of the 560 parent MTV-MOFs. The color bar denotes the averaged LCD of each family.

and thus the effect of enhanced interactions is negligible and (ii) additional functional groups occupy space, which reduces the $CO_2$ uptake. This is consistent with an experimental observation from Babarao and co-workers, where they reported that functionalized IRMOF-9 shows a reduction in $CO_2$ uptake at 298 K and 1 bar when compared with the parent IRMOF-9.[27] The authors showed that the pendent functional groups blocked $CO_2$ molecules from entering a small pore in the parent interpenetrated MOF that was the most favorable for $CO_2$ adsorption. It should be noted that the MOF exhibiting the highest $CO_2$ adsorption performance of one family may have a different combination type of functional groups from the top performer of another family (Table S2), implicating the minor role of the functional group combination, as shown in Figure 3.

The dependence of $CO_2$ capture performance on the LCD is depicted via color in Figure 4. In general, the larger the LCD of the MTV-MOFs, the smaller the enhancement in their $CO_2$ adsorption capacity and $CO_2/N_2$ selectivity. Specifically, there is little improvement in $CO_2$ capture performance upon functionalization for MOFs with LCDs above 12 Å, and for smaller LCDs, the enhancement in $CO_2$ adsorption capacity and selectivity becomes more apparent. The $CO_2$ adsorption capacity of functionalized MTV-MOFs can reach approximately twice that of the parent MOF when the LCD is below 12 Å. Figure 4a shows some evidence that when the average LCD values are below 6 Å (orange points), the enhancement in $CO_2$ uptake becomes marginal. This is because the pore space is already saturated with $CO_2$ molecules at the partial pressure of interest for MOFs with small pores, and additional functional


DOI: 10.1021/acs.jpclett.7b02700
J. Phys. Chem. Lett. 2017, 8, 6135−6141

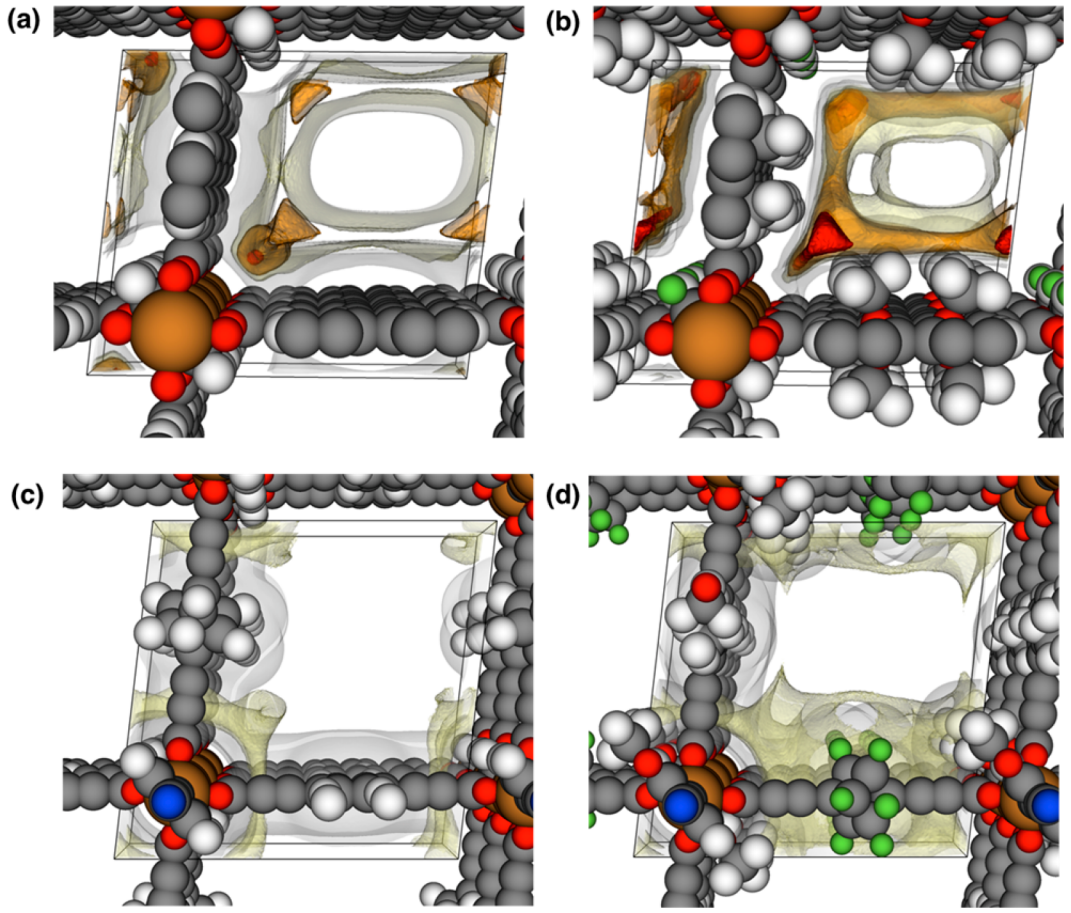


**Figure 5.** Excess free energy contour maps of representative parent MTV-MOFs (a,c) and functionalized MTV-MOF counterparts (b,d) with small (a,b) and large (c,d) pore sizes. The small-pore parent MTV-MOF (a) is composed of linkers 16C, 10C, and 4N, and its functionalized counterpart (b) is composed of the $-OCH_3$-functionalized 16C and 10C and −F-functionalized 4N. The large-pore parent MTV-MOF (c) consists of linkers 9C, 11C, and 7N, and its counterpart (d) consists of −F-functionalized 11C and $-OCH_3$-functionalized 9C and 7N. Red: −20 kJ/mol; orange: −15 kJ/mol; yellow: −10 kJ/mol; gray: 25 kJ/mol. Gray balls represent carbon, white: hydrogen, red: oxygen, blue: nitrogen, green: fluorine, orange: copper.

groups simply lead to reduced $CO_2$ uptake due to reduced pore volume or blockage of pores.[27] Considering the effect of pore size on the $CO_2/N_2$ selectivity in Figure 4b, the selectivity continues to increase for functionalized MTV-MOFs when compared with the parent structures even for small pore sizes, which is likely due to the increased potential well overlap in small pores.[28,29] From the structures that we generated, the highest enhanced $CO_2/N_2$ selectivity is approximately three times that of the parent MOF.

Figure S7a shows that the increase in $CO_2$ heat of adsorption upon functionalization also depends on the pore size. In general, we find that if the pore of the parent MOF is small (i.e., 7−11 Å), the functionalization leads to a large increase in the $CO_2$ heat of adsorption, adsorption capacity, and $CO_2/N_2$ selectivity. However, when the pore size of the parent MOF is less than 6 Å, functionalization reduces the $CO_2$ uptake because the pore volume decreases. Nevertheless, the $CO_2/N_2$ selectivity of functionalized MOFs increases with decreasing pore size in the materials studied here.

To illustrate the changes in the adsorbent−adsorbate interactions at specific sites within parent versus functionalized structures, we chose two representative pairs of parent and functionalized MTV-MOFs and computed the excess free energy landscape of an adsorbed $CO_2$ molecule (see Figure 5 and the SI for details). The parent MOF in the first pair of MTV-MOFs (Figure 5a,b) has a relatively small LCD (9.8 Å), and the parent for the second pair (Figure 5c,d) has a relatively large LCD (15.0 Å). For the small-pore MOF, we can see an increase in the volume of the attractive region (contours at −15 kJ/mol in orange, −10 kJ/mol in yellow) after functionalization. In addition, the adsorption sites at the metal corners (−20 kJ/mol in red) are significantly enhanced, and the affinity of the entire surface for $CO_2$ molecules becomes stronger. On the other hand, the free energy contour maps of parent and functionalized MTV-MOFs with the large pore (Figure 5c,d) show no highly attractive region (in red or orange) displayed in either framework. We see only a marginal influence of the functional groups on the internal environment for a $CO_2$ molecule in this framework through the slight increase in volume of the moderately attractive region (yellow). These pairs of examples visually underscore our observations in Figure 4.

In summary, we explored the chemical space of a class of MTV-MOFs by constructing a database of ∼10 000 hypothetical MTV-MOF structures with mixed linkers and mixed functional groups and conducted a high-throughput computational screening to identify high-performing candidates for $CO_2$ capture. Our results provide insights into the role of functional groups in $CO_2$ capture performance. We demonstrated that functionalization increases the $CO_2/N_2$ selectivity over the



DOI: 10.1021/acs.jpclett.7b02700
J. Phys. Chem. Lett. 2017, 8, 6135−6141

parent MOF in every case, and functionalization also increases the $CO_2$ capacity over the parent structure in most cases. The magnitude of the enhancement is more significant for MTV-MOFs with small pores. For MOFs whose pores are so small that adding functional groups occupies scarce space for a $CO_2$ molecule to sit or blocks accessibility to small pores present in the parent MOF, gas adsorption is reduced upon functionalization, as also found by Babarao et al.[27] This work reveals that the pore size and the size of the functional groups can be just as important as the chemical nature of the functional groups in determining the $CO_2$ adsorption performance of MTV-MOFs. This insight should be useful in choosing parent MOFs with suitable pore sizes when designing MTV-MOFs with improved performance. Although only **pcu** topology was considered in this work, we believe that our conclusions on the dominant role of the pore size will likely hold true for MTV-MOFs of other topologies. We make our database of MTV-MOF structures and corresponding simulated $CO_2$ uptakes openly available as SI to motivate the experimental synthesis and testing of top candidates for $CO_2$ capture.

## ■ ASSOCIATED CONTENT

### Supporting Information

The Supporting Information is available free of charge on the ACS Publications website at DOI: 10.1021/acs.jpclett.7b02700.

Detailed information for constructing the MTV-MOF database, simulation details, and additional supporting results (PDF)

Crystal structures of the MTV-MOF database in CIF format (ZIP)

## ■ AUTHOR INFORMATION


### Corresponding Author

*E-mail: snurr@northwestern.edu.

### ORCID

Yongchul G. Chung: 0000-0002-7756-0589

Randall Q. Snurr: 0000-0003-2925-9246


### Notes

The authors declare the following competing financial interest(s): R.Q.S. has a financial interest in the start-up company NuMat Technologies, which is seeking to commercialize metal-organic frameworks.

## ■ ACKNOWLEDGMENTS

This work was supported by the U.S. Department of Energy, Office of Basic Energy Sciences, Division of Chemical Sciences, Geosciences and Biosciences under Award DE-FG02-12ER16362. S.L. acknowledges support from the National Natural Science Foundation of China (NSFC) under Project No. 51606081. Y.G.C. acknowledges support from Basic Science Research Program through the National Research Foundation of Korea (NRF) funded by the Ministry of Education (NRF-2016R1D1A1B03934484). We thank the National Energy Research Scientific Computing Center (NERSC), which is supported by the Office of Science of the U.S. Department of Energy under Contract No. DE-AC02-05CH11231, for computational resources and the computational resources and staff contributions provided by the Quest high-performance computing facility at Northwestern University (Project Allocation: p20663), which is jointly supported by the Office of the Provost, the Office for Research, and Northwestern University Information Technology.

## ■ REFERENCES


(1) Furukawa, H.; Cordova, K. E.; O'Keeffe, M.; Yaghi, O. M. The Chemistry and Applications of Metal-Organic Frameworks. *Science* **2013**, *341*, 1230444.

(2) Kitaura, R.; Iwahori, F.; Matsuda, R.; Kitagawa, S.; Kubota, Y.; Takata, M.; Kobayashi, T. C. Rational Design and Crystal Structure Determination of a 3-D Metal-Organic Jungle-Gym-Like Open Framework. *Inorg. Chem.* **2004**, *43*, 6522−6524.

(3) Ma, B. Q.; Mulfort, K. L.; Hupp, J. T. Microporous Pillared Paddle-Wheel Frameworks Based on Mixed-Ligand Coordination of Zinc Ions. *Inorg. Chem.* **2005**, *44*, 4912−4914.

(4) Burrows, A. D. Mixed-Component Metal-Organic Frameworks (MC-MOFs): Enhancing Functionality through Solid Solution Formation and Surface Modifications. *CrystEngComm* **2011**, *13*, 3623−3642.

(5) Deng, H. X.; Doonan, C. J.; Furukawa, H.; Ferreira, R. B.; Towne, J.; Knobler, C. B.; Wang, B.; Yaghi, O. M. Multiple Functional Groups of Varying Ratios in Metal-Organic Frameworks. *Science* **2010**, *327*, 846−850.

(6) Wang, L. J.; Deng, H. X.; Furukawa, H.; Gandara, F.; Cordova, K. E.; Peri, D.; Yaghi, O. M. Synthesis and Characterization of Metal-Organic Framework-74 Containing 2, 4, 6, 8, and 10 Different Metals. *Inorg. Chem.* **2014**, *53*, 5881−5883.

(7) Kong, X. Q.; Deng, H. X.; Yan, F. Y.; Kim, J.; Swisher, J. A.; Smit, B.; Yaghi, O. M.; Reimer, J. A. Mapping of Functional Groups in Metal-Organic Frameworks. *Science* **2013**, *341*, 882−885.

(8) Katzenmeyer, A. M.; Canivet, J.; Holland, G.; Farrusseng, D.; Centrone, A. Assessing Chemical Heterogeneity at the Nanoscale in Mixed-Ligand Metal-Organic Frameworks with the PTIR Technique. *Angew. Chem., Int. Ed.* **2014**, *53*, 2852−2856.

(9) Jayachandrababu, K. C.; Verploegh, R. J.; Leisen, J.; Nieuwendaal, R. C.; Sholl, D. S.; Nair, S. Structure Elucidation of Mixed-Linker Zeolitic Imidazolate Frameworks by Solid-State H-1 CRAMPS NMR Spectroscopy and Computational Modeling. *J. Am. Chem. Soc.* **2016**, *138*, 7325−7336.

(10) Taddei, M.; Tiana, D.; Casati, N.; van Bokhoven, J. A.; Smit, B.; Ranocchiari, M. Mixed-Linker UiO-66: Structure-Property Relationships Revealed by a Combination of High-Resolution Powder X-Ray Diffraction and Density Functional Theory Calculations. *Phys. Chem. Chem. Phys.* **2017**, *19*, 1551−1559.

(11) Han, S. S.; Kim, D.; Jung, D. H.; Cho, S.; Choi, S. H.; Jung, Y. Accurate Ab Initio-Based Force Field for Predictive $CO_2$ Uptake Simulations in MOFs and ZIFs: Development and Applications for MTV-MOFs. *J. Phys. Chem. C* **2012**, *116*, 20254−20261.

(12) Drummond, M. L.; Cundari, T. R.; Wilson, A. K. Cooperative Carbon Capture Capabilities in Multivariate MOFs Decorated with Amino Acid Side Chains: A Computational Study. *J. Phys. Chem. C* **2013**, *117*, 14717−14722.

(13) McDaniel, J. G.; Yu, K.; Schmidt, J. R. Microscopic Origins of Enhanced Gas Adsorption and Selectivity in Mixed-Linker Metal-Organic Frameworks. *J. Phys. Chem. C* **2013**, *117*, 17131−17142.

(14) Zhang, Y. B.; Furukawa, H.; Ko, N.; Nie, W. X.; Park, H. J.; Okajima, S.; Cordova, K. E.; Deng, H. X.; Kim, J.; Yaghi, O. M. Introduction of Functionality, Selection of Topology, and Enhancement of Gas Adsorption in Multivariate Metal Organic Framework-177. *J. Am. Chem. Soc.* **2015**, *137*, 2641−2650.

(15) Yuan, S.; Lu, W. G.; Chen, Y. P.; Zhang, Q.; Liu, T. F.; Feng, D. W.; Wang, X.; Qin, J. S.; Zhou, H. C. Sequential Linker Installation: Precise Placement of Functional Groups in Multivariate Metal-Organic Frameworks. *J. Am. Chem. Soc.* **2015**, *137*, 3177−3180.

(16) Yuan, S.; Chen, Y. P.; Qin, J. S.; Lu, W. G.; Zou, L. F.; Zhang, Q.; Wang, X.; Sun, X.; Zhou, H. C. Linker Installation: Engineering Pore Environment with Precisely Placed Functionalities in Zirconium MOFs. *J. Am. Chem. Soc.* **2016**, *138*, 8912−8919.




DOI: 10.1021/acs.jpclett.7b02700
*J. Phys. Chem. Lett.* 2017, 8, 6135−6141

(17) Liu, L. J.; Konstas, K.; Hill, M. R.; Telfer, S. G. Programmed Pore Architectures in Modular Quaternary Metal-Organic Frameworks. *J. Am. Chem. Soc.* **2013**, *135*, 17731−17734.
(18) Wilmer, C. E.; Farha, O. K.; Bae, Y. S.; Hupp, J. T.; Snurr, R. Q. Structure-Property Relationships of Porous Materials for Carbon Dioxide Separation and Capture. *Energy Environ. Sci.* **2012**, *5*, 9849−9856.
(19) Han, S. G.; Huang, Y. G.; Watanabe, T.; Dai, Y.; Walton, K. S.; Nair, S.; Sholl, D. S.; Meredith, J. C. High-Throughput Screening of Metal-Organic Frameworks for $CO_2$ Separation. *ACS Comb. Sci.* **2012**, *14*, 263−267.
(20) Sun, W. Z.; Lin, L. C.; Peng, X.; Smit, B. Computational Screening of Porous Metal-Organic Frameworks and Zeolites for the Removal of $SO_2$ and $NO_x$ from Flue Gases. *AIChE J.* **2014**, *60*, 2314−2323.
(21) Wilmer, C. E.; Leaf, M.; Lee, C. Y.; Farha, O. K.; Hauser, B. G.; Hupp, J. T.; Snurr, R. Q. Large-Scale Screening of Hypothetical Metal-Organic Frameworks. *Nat. Chem.* **2012**, *4*, 83−89.
(22) Colon, Y. J.; Fairen-Jimenez, D.; Wilmer, C. E.; Snurr, R. Q. High-Throughput Screening of Porous Crystalline Materials for Hydrogen Storage Capacity near Room Temperature. *J. Phys. Chem. C* **2014**, *118*, 5383−5389.
(23) Banerjee, D.; Cairns, A. J.; Liu, J.; Motkuri, R. K.; Nune, S. K.; Fernandez, C. A.; Krishna, R.; Strachan, D. M.; Thallapally, P. K. Potential of Metal-Organic Frameworks for Separation of Xenon and Krypton. *Acc. Chem. Res.* **2015**, *48*, 211−219.
(24) Sikora, B. J.; Wilmer, C. E.; Greenfield, M. L.; Snurr, R. Q. Thermodynamic Analysis of Xe/Kr Selectivity in over 137 000 Hypothetical Metal-Organic Frameworks. *Chem. Sci.* **2012**, *3*, 2217−2223.
(25) Huang, H. L.; Zhang, W. J.; Yang, F.; Wang, B.; Yang, Q. Y.; Xie, Y. B.; Zhong, C. L.; Li, J. R. Enhancing $CO_2$ Adsorption and Separation Ability of Zr(IV)-Based Metal-Organic Frameworks through Ligand Functionalization under the Guidance of the Quantitative Structure-Property Relationship Model. *Chem. Eng. J.* **2016**, *289*, 247−253.
(26) Banerjee, R.; Furukawa, H.; Britt, D.; Knobler, C.; O'Keeffe, M.; Yaghi, O. M. Control of Pore Size and Functionality in Isoreticular Zeolitic Imidazolate Frameworks and Their Carbon Dioxide Selective Capture Properties. *J. Am. Chem. Soc.* **2009**, *131*, 3875−3877.
(27) Babarao, R.; Coghlan, C. J.; Rankine, D.; Bloch, W. M.; Gransbury, G. K.; Sato, H.; Kitagawa, S.; Sumby, C. J.; Hill, M. R.; Doonan, C. J. Does Functionalisation Enhance $CO_2$ Uptake in Interpenetrated MOFs? An Examination of the IRMOF-9 Series. *Chem. Commun.* **2014**, *50*, 3238−3241.
(28) Gomez, D. A.; Combariza, A. F.; Sastre, G. Confinement Effects in the Hydrogen Adsorption on Paddle Wheel Containing Metal-Organic Frameworks. *Phys. Chem. Chem. Phys.* **2012**, *14*, 2508−2517.
(29) Burtch, N. C.; Jasuja, H.; Dubbeldam, D.; Walton, K. S. Molecular-Level Insight into Unusual Low Pressure $CO_2$ Affinity in Pillared Metal-Organic Frameworks. *J. Am. Chem. Soc.* **2013**, *135*, 7172−7180.



DOI: 10.1021/acs.jpclett.7b02700
*J. Phys. Chem. Lett.* 2017, 8, 6135−6141